Ultrafast erbium doped fiber laser modulated by Nb_4AlC_3 saturable absorber

Xiao-juan Liu*, Mei-Xia Zhang, Tian-run Liu, Wen-hao Lv, Cheng Lu*

(Shandong University of Technology, School of Physics and Optoelectronic Engineering, Zibo, Shandong 255049, P.R. China)

**Corresponding Author, E-mail: liuxiaojuansd@163.com; luchengcg@163.com*

Abstract: Conventional soliton (CS) mode-locked erbium-doped fiber (EDF) laser is realized by MAX phases material (MAX-PM) of Nb_4AlC_3 as saturable absorber (SA). First, liquid phase exfoliation (LPE) method is utilized to prepare Nb_4AlC_3 nanosheets, and then, a piece of taper-fiber is adopted to fabricate Nb_4AlC_3-SA. The saturation intensity and modulation depth of the Nb_4AlC_3-SA are 2.02 MW/cm^2 and 1.88 %. Based on the Nb_4AlC_3-SA, conventional soliton (CS) mode-locked EDF laser is achieved. The central wavelength, pulse duration, and pulse repetition rate are 1565.65 nm, 615.37 fs, and 24.63 MHz, respectively. The performance are competitive and particularly superior in terms of pulse duration. To the best of our knowledge, this is the first report of Nb_4AlC_3 material is used as modulator for ultrafast pulse generation. The work fully confirms that Nb_4AlC_3 possesses marvellous nonlinear saturable absorption property, as well broadens new avenues and opportunities for further research of air-stable ultrafast photonic devices.

Key words: Conventional soliton (CS); Nb_4AlC_3; Erbium-doped fiber (EDF) laser; Saturable absorber (SA)

基于 Nb_4AlC_3可饱和吸收体的超快掺铒光纤激光器

刘晓娟*，张美霞，刘天润，吕文豪，鲁成*

（山东理工大学物理与光电工程学院，山东省淄博市，255049）

摘要：本文采用 MAX 相（MAX-PM）材料 Nb_4AlC_3作为可饱和吸收体（SA），实现了传统孤子（CS）锁模掺铒光纤（EDF）激光器。首先，利用液相剥离（LPE）法制备了 Nb_4AlC_3纳米片，然后采用拉锥光纤制作了 Nb_4AlC_3-SA。该 Nb_4AlC_3可饱和吸收体的饱和强度和调制深度分别为 2.02 MW/cm²和 1.88%。基于所制备的 Nb_4AlC_3可饱和吸收体，实现了传统孤子锁模掺铒光纤激光器。该激光器的中心波长、脉冲持续时间和脉冲重复率分别为 1565.65 nm、615.37 fs 和 24.63 MHz。该锁模激光器性能优越，特别是在脉冲持续时间方面表现优异。据我们所知，这是首次将 Nb_4AlC_3材料用作可饱和吸收体实现超快脉冲光纤激光器的报道。本研究充分证实 Nb_4AlC_3具有优异的非线性可饱和吸收特性，同时也为空间稳定型超快光子器件的深入研究拓宽了途径。

关键词：传统孤子 (CS); Nb_4AlC_3; 掺铒光纤 (EDF) 激光器; 可饱和吸收体 (SA)

中图分类号：TN248

收稿日期: XXXXX; **修订日期:** XXXXX

基金项目: 山东淄博市校城融合项目(2019ZBXC120)

Supported by the Shandong University of Technology and Zibo City Integration Development Project (2019ZBXC120).

1. Introduction

Ultrafast fiber lasers, possessing ultra-short pulse duration and ultra-high peak-power, have found significant applications in optical communication, medical diagnostics, precision measurement, astronomical detection, fundamental scientific research, and so on [1-4]. Among the available ultrafast pulse generation technologies, passively mode-locked fiber laser based on saturable absorber (SA) has become one of the most effective methods due to its advantages of compact structure, low cost, and good compatibility [5-10].

From the SA point of view, numerous SAs have been explored to conduct mode-locked operations. Some are effective SAs, such as nonlinear polarization rotation (NPR) [5], nonlinear optical loop mirror (NOLM) [7] and nonlinear Kerr effect [8, 9]. Others are real SAs such as semiconductor saturable absorber mirror (SESAM) [10], SAs based on two dimensional (2D) materials including but not limited to single-walled carbon nanotubes [5], graphene [6], and other 2D layered materials [11-15]. It is undeniable that each individual SA always coexists with advantages and disadvantages. Among them, NPR and NOLM have all-fiber structure and is capable of sustaining higher light intensity. However, the pump power threshold for mode-locked operation is high. Besides, they are highly sensitive to the environment disturbance, which results in low system stability and limits its practical applications. Comparatively, SESAM is one of the most successfully commercialized real SA devices so far. However, SESAM suffers from high cost, complex preparation, limited operating bandwidth and low damage threshold [6, 10]. Fortunately, spurred by the advent of graphene [16, 17], a wide range of 2D materials have been recognized and demonstrated to be excellent SAs. Sufficient researches have shown that the application of 2D material-SAs as broadband, cost-efficient, and widely used optical modulators for ultrafast lasers generation is a high-speed developing field with broad commercial prospects [18-21].

MAX phases materials (MAX-PM) are layered ternary carbides or nitrides with ceramic and metallic properties [22-26]. Generally, the formula for MAX-PM is $M_{n+1}AX_n$, where M represents one kind of transition metals such as Sc, Ti, Zr, Hf, V, Nb, Ta, Cr, Mo, etc. X is a carbon or/and nitrogen with n = 1, 2, 3, and A represents an element belongs to group III, IV, V, or VI such as Al, Ga, In, Si, Ge, Sn, P, As, S, etc.. Besides, the structure of MAX-PM is characterized by alternating layers of M and A atoms, forming an almost tightly packed hexagonal layered structure with X atoms filling octahedral voids. Due to the special atomic arrangement, MAX-PM is actually a combination of metal and ceramic. In its ceramic state, MAX-PM presents exceptional resistance to oxidation and high temperature. Conversely, in its metallic state, it showcases high-temperature plasticity as well as excellent electrical and thermal conductivity. These hybrid characteristics make it highly desirable for applications in nuclear engineering, high-temperature devices, and the aerospace industry. On the other hand, the emergence of MAX-PM has undoubtedly promoted the development of SAs. The excellent nonlinear saturable absorption features such as impressive modulation depth, flexibly tunable bandgap, and high electron density around Fermi level make MAX-PM formidable contender in the SA family [27-32]. In particular, Nb_4AlC_3 is a member of MAX-PM family. In addition to the commonality of MAX-PM, the valence and conduction bands of the Nb_4AlC_3 overlap greatly, and the band gap at Fermi energy level is zero. Such properties endow Nb_4AlC_3 with good

photoelectric response property [27, 29]. Furthermore, Nb_4AlC_3 is gifted with high antioxidant property by the formation of a protective layer due to atmospheric oxidation of aluminum inside the Nb_4AlC_3 [26-28]. Taking the above analysis into account, an environmentally stable Nb_4AlC_3 based optoelectronic device is expected. However, Nb_4AlC_3 material has rarely been researched in the field of nonlinear optics so far.

In this work, passively mode-locked erbium-doped fiber (EDF) lasers is successfully modulated by taper-fiber-structured Nb_4AlC_3-SA. The Nb_4AlC_3 dispersion is prepared by LPE method. Then taper-fiber-structured Nb_4AlC_3-SA is fabricated and the saturation intensity and modulation depth of the prepared are tested to be 2.02 MW/cm^2 and 1.88%. Conventional soliton (CS) mode-locked EDF laser is achieved with output central wavelength, pulse duration and pulse repetition rate of 1565.65 nm, 615.37 fs and 24.63 MHz, respectively. To the best of our knowledge, this is the first report of Nb_4AlC_3-SA applied as a mode-locker. The work confirms that Nb_4AlC_3 possesses excellent nonlinear saturable absorption property and outstanding modulation capability, as well provides valuable references for further research of air-stable ultrafast photonic devices with Nb_4AlC_3 materials.

2. Fabrication and characterization of taper-fiber-structured Nb_4AlC_3-SA

In recent years, top-down or bottom-up methods including micromechanical exfoliation (ME), chemical vapor deposition (CVD), Liquid-phase exfoliation (LPE) have been successfully applied to prepare mono- or few-layer 2D material nanosheets [33-36]. Each method has its advantage and limitation in practical applications. ME is capable of producing any kind 2D material nanosheets with high-quality, its disadvantage is that the production efficiency and size are limited. CVD, a bottom-up preparation method, could synthesize large-scale monosheets film with high purity, large area, and uniform thickness. However, the method has high cost and complexity, and the preparation is often accompanied by the follow-up process of film transfer. LPE, always assisted by high-intensity ultrasonication, is a simple and cost-effective method to fabricate nanosheets at ambient conditions. For LPE method, forceful solvent-2D nanoflake-interaction (internal force) and sonication energy (external force) are critical factors for the exfoliation efficiency [34, 35]. In this article, the Nb_4AlC_3 nanosheets are prepared by LPE method.

Taper fibers are widely adopted to fabricate SA devices. On the one hand, by changing the size and structure in the tapering process, high dispersion and nonlinearity of optical fiber can be introduced, which facilitates the laser system to efficiently compress pulse duration [37-39]. On the other hand, large-area thin 2D nanosheet film integrated with taper fiber structure can offer tight optical confinement for enhancing the light-material interaction, hence the modulation effect is strengthened. Besides, the utilization of the evanescent field of the taper fiber protects the 2D material SA from thermal damage.

In this work, to obtain the taper-fiber-structured Nb_4AlC_3-SA for the proposed mode-locking, first, the Nb_4AlC_3 nanosheets are prepared by LPE method, and a taper-fiber is processed from a piece of commercial fiber (SM-28). Then, the SA is fabricated by coating the Nb_4AlC_3 nanosheets onto the twist part of the taper fiber. As the beginning, 20 ml deionized water is mixed with 10 mg Nb_4AlC_3 powder, then the mixture undergoes ultrasonication with repetition rate and

power of 40 kHz and 300 W at room temperature of 25 ℃ for 12 h. The as-prepared Nb_4AlC_3 solution subsequently undergoes a high-speed centrifugation process at 1500 rpm for 10 min. The 70% supernatant is collected for characterization and SA fabrication. The taper fiber, same to our previous work [39], is fabricated by a hydrogen-oxygen flame-based fiber processing machine from a piece of standard single-mode fiber (SM 28). The waist diameter of 15 μm and tapered length of 1 cm are precisely controlled by the preset program. Then, using a home-made fiber holder, the tapered part is exposed in ambient air, kept rotating vertically to the direction of the optical fiber and tilting repeatedly along the fiber direction simultaneously. After the as-prepared Nb_4AlC_3 nanosheets supernatant is slowly dropped onto the surface of the waist area and evaporated to dryness, a taper-fiber-structured Nb_4AlC_3-SA is obtained.

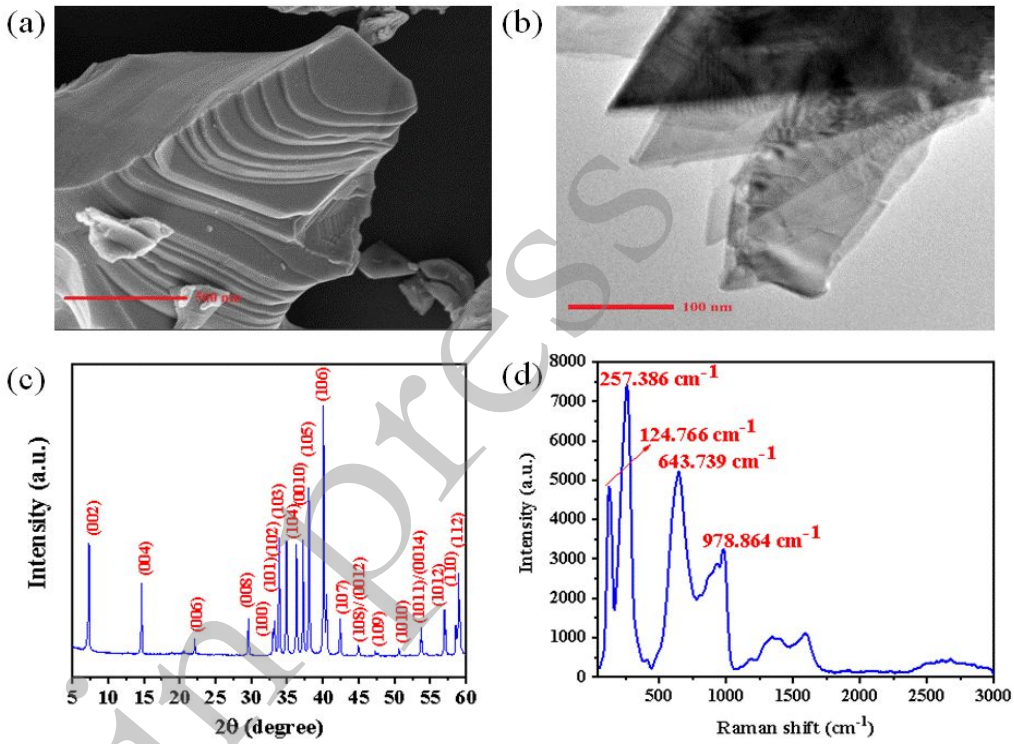

Fig. 1. Properties of the Nb_4AlC_3 nanosheets. (a) SEM image. (b) TEM image. (c) XRD pattern. (d) Raman spectrum.

Subsequently, the Nb_4AlC_3 nanosheets are characterized. Fig. 1(a) depicts the scanning electron microscopy (SEM) (Czech Republic TESCAN MIRA LMS) with a resolution of 500 nm. The surface texture reveals a good laminar structure. Fig. 1(b) presents the transmission electron microscope (TEM) (Japan JEOL JEM 2800). The clear lattice structure confirms the successful exfoliation of the Nb_4AlC_3 powder. The X-ray diffraction (XRD) (AXS D8 Advance, Bruker, Billerica, MA, USA) pattern is shown in Fig. 1(c). It's seen that all diffraction peaks are consistent with previous reports [28, 31], which confirms the Nb_4AlC_3 truth of the sample. Raman spectroscopy is able to effectively distinguish different substances or accurately identify the constituents of substances, so the Raman spectrum of the Nb_4AlC_3 sample is tested and shown in Fig. 1(d). The four typical peaks of the Nb_4AlC_3 sample is apparent and analogous to the previous report [29, 32, 40].

The intensity dependent nonlinear saturable absorption property of Nb_4AlC_3-SA is investigated by a balanced twin-detector. As shown in Fig. 2(a), a home-made fiber laser with center wavelength, pulse duration and repetition rate of 1560 nm, 500 fs and 10 MHz is used as the light source. After an attenuator, the injected light is equally divided into two beams by an 50/50 optical coupler. The signal light passing through Nb_4AlC_3-SA is tested by power meter I, while the reference light is tested by power meter II. The data are recorded and shown as blue dots in Fig. 2(b). It's observed that the transmission efficiency of the SA increases with pulse intensity, which is the typical characteristic of nonlinear saturable absorption. When the light intensity reaches 1.35 MW/cm^2, the transmission reaches the maximum, indicating the saturation of the SA. The saturation intensity and modulation depth can be determined by the formula [41]:

$$T(I) = 1 - T_{ns} - \Delta T * \exp\left(-\frac{I}{I_{sat}}\right) \quad (1)$$

where $T(I)$ and ΔT are the transmission and the modulation depth, I and I_{sat} are the laser intensity and the saturation intensity, T_{ns} is the non-saturable loss. At last, the saturation intensity and modulation depth of the prepared SA are deduced to be 2.02 MW/cm^2 and 1.88 %.

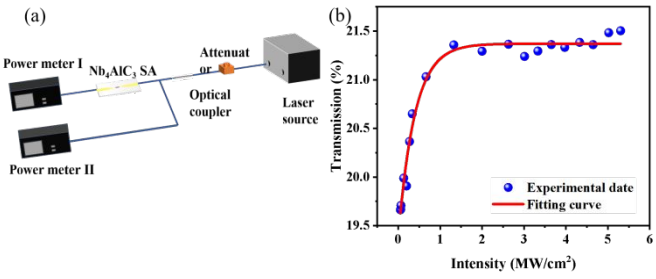

Fig. 2. (a) Balanced twin-detector for measuring saturable absorption properties. (b) Nonlinear saturable absorption property of Nb_4AlC_3-SA.

The characterization results demonstrated above provide a good understanding of the optical nonlinearity properties of Nb_4AlC_3 nanosheets. The exploration is a good reference to further development in photonics and photoelectric applications of Nb_4AlC_3 materials.

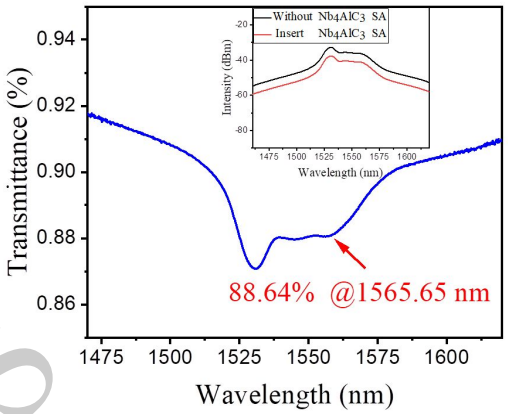

Fig. 3. Linear transmittance of the fabricated taper-fiber structured Nb_4AlC_3-SA.

Using the same detector in [39], the linear transmittance of the prepared Nb_4AlC_3-SA is studied and depicted in Fig. 3. The black curve and the red curve in the inset are the output ASE spectra without and with Nb_4AlC_3-SA inserted into the optical path, respectively. The quotient of the former data divided by the latter data is the linear transmittance, which is presented as blue curve. Ultimately, the linear transmittance at 1565.65 nm is determined to be 88.64%, indicating that the prepared SA is suitable to be used as photonics devices with low insertion loss.

3. Experimental setup

The alignment-free experimental setup of the mode-locked EDF laser using Nb_4AlC_3-SA as modulator is schematically depicted in Fig. 4. It has a ring cavity configuration with a total length of about 8.4 m. A 980 nm LD with a maximum output power of 500 mW is employed as a pump source, and a 980/1550 nm wavelength division multiplexer (WDM) is used to

couple the pump light into the cavity. An in-line polarization controller (PC) is used to fine tune the birefringence environment or adjust the polarization state of the cavity, but it is not fundamental to realize the mode locking operation. In addition, a polarization-independent isolator (PI-ISO) is used to ensure unidirectional running of the laser. A piece of 40-cm-long EDF (Liekki Er-110-4/125) with a dispersion parameter of -46 ps/nm/km is used as the gain medium. The net dispersion of the whole ring cavity is calculated to be about -0.15 ps^2, which facilitates CS pulse shaping through the interaction of self-phase modulation and anomalous group velocity dispersion (GVD). 10 % of the signal is extracted outside the cavity by an optical coupler (OC). The output performance is monitored by a digital oscilloscope (OSC) (Wavesurfer 3054, LeCroy, Teledyne, USA) with a 3-GHz photo-detector (PD 03), an optical spectrum analyzer (OSA) (AQ6370B, Yokogawa, Tokyo, Japan), a radio frequency spectrum analyzer (FPC1000, Rohde & Schwarz, Jena, Germany) and a power meter (PM3, Molectron, Barrington, NJ, USA). The pulse duration is measured by an optical autocorrelator (AC) (Femtochrome FR-103 XL, Berkeley, USA).

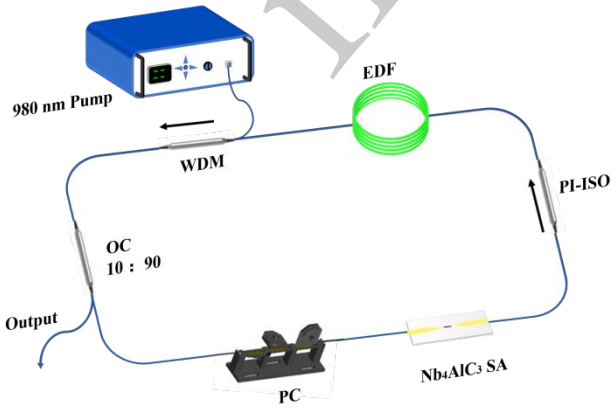

Fig. 4. Experimental setup of mode-locked EDF laser based on Nb_4AlC_3-SA.

4. Experimental results and discussion

When the Nb_4AlC_3-SA is absent from the cavity, the system only operates in continuous wave (CW) regime in the full adjustment range of the PC and pump power, which means that the current devices involved in the ring cavity can not provide enough modulation for pulse generation. By incorporating the taper-fiber-structured Nb_4AlC_3-SA into the ring cavity, with the PC's orientations being fine tuned and the pump power being increased beyond the mode-locked threshold, the system evolves into CS operation on its own (called self-starting) and keeps stable in the pump power range of 100-340 mW.

Fig. 5 shows the spectral and temporal performance of the CS operation. As illustrated by Fig. 5(a), the out spectrum centered at 1565.65 nm with a 3 dB bandwidth of 7.78 nm. Several pairs of Kelly sidebands symmetrically distribute on both sides of the center wavelength, verifying the typical CS characteristics. The formation mechanism of the Kelly sidebands is studied and explained that the losses existing in the laser cavity promote the generation of dispersion wave, and when the phase difference between the soliton and the dispersion wave reaches 2π, strong interference occurs and Kelly sidebands are generated. The wavelength location of the Kelly sidebands usually matches with the dispersion by the following formula [42]:

$$\Delta\lambda = \frac{\lambda^2}{0.576\pi c\tau}\sqrt{-1+\frac{4\pi(0.5657\tau)^2}{k''L}} \quad (2)$$

where c is the velocity of light (the same in the following (3) and (4)), k'' is the average GVD of the total cavity, L is the cavity length, τ is the half-height full width of the pulse, $\Delta\lambda$ is the wavelength offset of Kelly sideband from the center wavelength of the CS, and λ is the central wavelength of the CS spectrum. The spectral interval $\Delta\lambda$ is inversely proportional to the

net dispersion of the resonant cavity, which indicates that when the net dispersion of the cavity gradually approaches zero, the $\Delta\lambda$ gradually becomes wider and eventually exceeds the gain spectral bandwidth. Consequently stretched soliton (SS) with square spectral top will be generated.

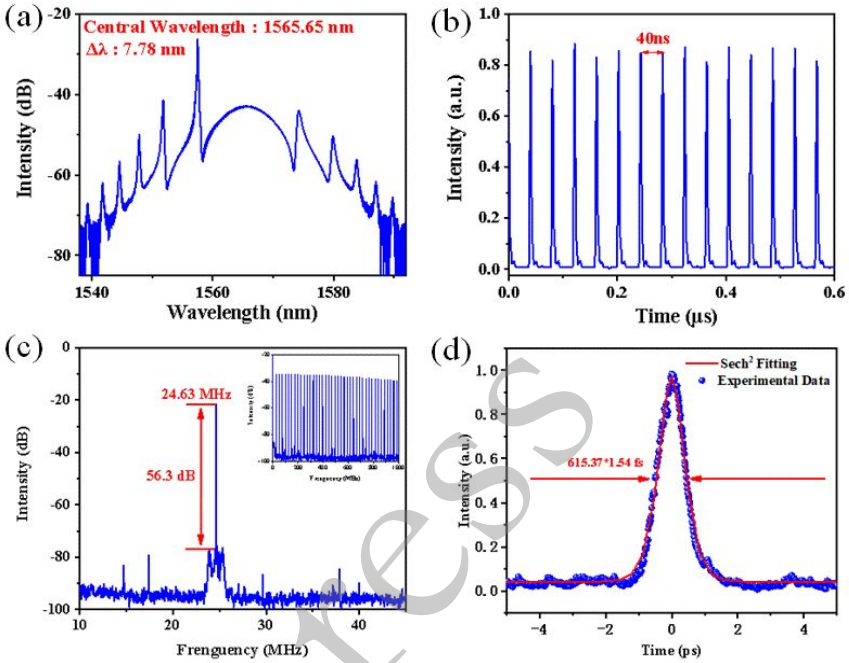

Fig. 5. Conventional soliton (CS) operation. (a) Spectrum. (b) Pulse trains. (c) RF spectrum. (d) Autocorrelation trace.

The pulse sequence within 600 ns is recorded and presented in Fig. 5(b). The temporal interval between adjacent pulses is 40 ns, which is well confirmed by the repetition rate of 24.63 MHz (f=1/T) in the RF spectra depicted in Fig. 5(c). The measured signal-to-noise ratio (SNR) is 56.3 dB, combining the broadband RF spectrum with a good flatness shown as inset in Fig. 5(c), depicts the high stability of the mode-locked operation. According to the following formula:

$$L = \frac{c}{nf} \tag{3}$$

where n, L, and f are the refractive index, cavity length, and the CS pulse repetition rate, respectively, the cavity length is theoretically calculated to be 8.34 m which keeps consistent with the actual length of 8.4 m.

As presented in Fig. 5(d), with a sech^2 pulse profile fitting, the pulse duration is determined to be 615.37 fs. According to the formula:

$$TBP = \frac{c\Delta\lambda\Delta t}{\lambda^2} \tag{4}$$

where λ, $\Delta\lambda$ and Δt are center wavelength, 3 dB bandwidth and pulse duration of the CS, respectively, the time-bandwidth product (TBP) is calculated to be 0.585, meaning the existence of chirp.

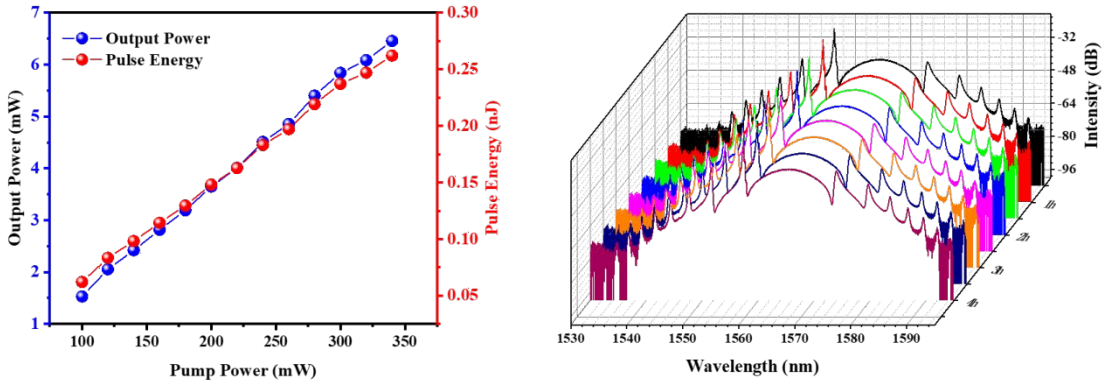

Fig. 6. (a) Output power and pulse energy vs. pump power. (b) Long-term stability of the laser system.

Fig. 6(a) illustrates that both the average output power and the pulse energy maintain a linear growth trend with the increase of pump power. At the pump power of 340 mW, the average output power reaches 6.45 mW, corresponding to a pulse energy of 0.262 nJ. To further confirm the long-term stability of the laser system, the output spectra at the highest power level are monitored in a time duration of 4 h with an interval of 30 min. As shown in Fig. 6(b), there is no apparent changes observed, so the system possesses excellent stability at room temperature.

Table 1 - Comparison of EDF lasers mode locked by various MAX-PM-based SAs.

SAs	Modulation depth (ΔT) (%)	Repetition rate (f) (MHz)	3 dB bandwidth ($\Delta\lambda$) (nm)	Pulse duration (Δt) (ps)	SNR (dB)	Output power (mW)	Refs
Ti_2CT_x	15.7	8.25	3.4	5.3	62	6.95	[43]
$Ti_3C_2T_x$	0.96	218.36	3.51	0.85	36	~ 1	[44]
V_2CT_x	3.1	1010.0	3.1	0.94	55	~ 25	[45]
Ti_3AlC_2	2	1.89	0.7	3.68	52.3	15.38	[46]
Ti_2AlC	2.21	16.7	3.8	0.68	64.6	2.7	[47]
V_2AlC	18	14.98	3.4	0.85	58	3.95	[48]
Nb_2AlC	2.62	58.6	0.2	5.8	58	2.07	[49]
Nb_4AlC_3	1.88	24.63	7.78	0.615	56.2	6.45	Our work

A relatively comprehensive comparison of current and previous MAX-PM mode-locked EDF lasers is summarized and listed in Table 1. It can be seen that our work reveals superior performance, particularly outstanding in terms of pulse duration. The results demonstrate the feasibility of Nb_4AlC_3-SA used as mode-locker in fiber lasers, which kisses well with our original expectation.

In the experiment, by using pure taper-fiber (directly exposed to the air) or removing the Nb_4AlC_3 SA, CW is always observed despite that the PC and the pump power are tuned over the full range. In contrast, modulated operation is ready to be achieved by depositing the Nb_4AlC_3 nanosheets on taper fiber. Besides, during the experiment, there is no additional nonlinear response from other devices is observed. These results declare that the saturable absorption property is purely caused by the as-prepared Nb_4AlC_3-SA.

Additionally, in our experiment, although the mode-locking phenomenon disappears at higher pump power than 340 mW, when the pump power is modulated from 500 mW back into the range of 100-340 mW, the mode-locking always recovers. Such results verify that the bleaching pump power of the Nb_4AlC_3-SA is around 340 mW, and the optical damage threshold of the Nb_4AlC_3-Sa is much higher.

Based on the taper-fiber-structured Nb_4AlC_3-SA, a stable CS mode-locked EDF laser is obtained with pulse duration of 615.37 fs. To the best of our knowledge, this is the first report of Nb_4AlC_3 material being used as mode-locker. The work systematically verifies that Nb_4AlC_3-SA possesses excellent nonlinear saturable absorption property, besides, broadens and inspires the avenues for further exploration of SAs.

5. Conclusion

References

[1] Debeuf M P, Knoops K, López-Iglesias C, *et al*.. Long-term remission of Hailey-Hailey disease by Er:YAG ablative laser therapy [J], *Journal of the European Academy of Dermatology and Venereolog*, 2024:03849989.

[2] Casamenti E, Pollonghini S, Bellouard Y, *et al*.. Few pulses femtosecond laser exposure for high efficiency 3D glass micromachining [J], *Optics Express*, 2021, 2 (22): 35054-35066.

[3] Hui Z Q, Bu X F, Wang Y H, *et al*.. Bi_2O_2Te Nanosheets Saturable Absorber-Based Passive Mode-Locked Fiber Laser: From Soliton Molecules to Harmonic Soliton. *Adv. Optical Mater*. 2022, 10: 2201812..

[4] Xing X W, Liu Y X, Han J F, *et al*.. Preparation of High Damage Threshold Device Based on Bi_2Se_3 Film and Its Application in Fiber Lasers[J], *ACS Photonics*, 2023, 10 (7).

[5] Nishizawa N, Kitajima S, Sakakibara Y, *et al*.. Spectral peaking in an ultrashort-pulse fiber laser oscillator with a molecular gas cell [J], *Optics Letters*, 2022, 47(10): 2422-2425.

[6] Keller U. Recent developments in compact ultrafast lasers[J], *Nature*, 2003, 424 (6950):831-838.

[7] HAN Y, GUO Y B, GAO B, *et al*..Generation, optimization, and application of ultrashort femtosecond pulse in mode-locked fiber lasers[J], *Progress in Quantum Electronics*, 2020, 71:100264.

[8] Renninger W H, Chong A, Wise F W, *et al*.. Giant-chirp oscillators for short-pulse fiber amplifiers[J], *Optics Letters*, 2008, 33 (24):3025-3027.

[9] YUN L, LIU X M. Generation and propagation of bound-state pulses in a passively mode-locked figure-eight laser[J], *IEEE Photonics Journal*, 2012, 4 (2):512-519.

[10]CUI Y D, LIU X M. Graphene and nanotube mode-locked fiber laser emitting dissipative and conventional solitons[J], *Optics Express*, 2013, 21(16):18969-18974.

[11] YANG Y, WANG CH R, HAN M M, et al.. Wavelength Convertible Flat/Tilt-Top Dissipative- Soliton-Resonance Pulses in an Anomalous Dispersion Fiber Laser [J], *Journal of Lightwave Technology*, 2024, 42(19): 6925 - 6931.

[12] HAN D D, MEI L ZH, HUI ZH Q, et al.. Flexible wavelength-, pulse-controlled mode-locked all-fiber laser based on a fiber Lyot filter [J], *Optics Express*, 2022, 30 (23): 41271-41278.

[13] LIU X, CHU H W, XU M J, *et al*.. Reverse saturable absorption in Ti3C2 MXene nanosheets for dissipative soliton resonance mode-locking operation in Er-doped fiber laser [J], *Optical Materials*, 2023, 136: 113463.

[14] SHANG X X, XU N N, GUO J, *et al*.. Nonlinear optical response of niobium telluride and its application for demonstrating pulsed fiber lasers [J], *Journal of Materiomics*, 2024, 10 (2):355-365.

[15] Li L, Xue Z, Liu W J, *et al*.. Saturable absorption properties and ultrafast photonics applications of HfS_3[J]. *Optics Letters*, 2024, 49(5): 1293-1296.

[16] ZHANG H, BAO Q L, TANG D Y, *et al*.. Large energy soliton erbium-doped fiber laser with a graphene-polymer composite mode locker[J], *Applied Physics Letters*, 2009, 95 (14): 141103.

[17] WANG L R, LIU X M, GONG Y K, *et al*.. Giant-chirp oscillator for ultra-large net-normal-dispersion fiber lasers[J], *Laser Physics Letters*, 2010, 7 (1):63-67.

[18] CHENG C H, LIN G R. Carbon Nanomaterials Based Saturable Absorbers for Ultrafast Passive Mode-Locking of Fiber Lasers [J], *Current Nanoscience*, 2020, 16(3): 441-457.

[19] ZHANG XU, XING X W, LI J, *et al*.. Controllable epitaxy of quasi-one-dimensional topological insulator α-Bi4Br4 for the application of saturable absorber [J], *Applied Physics Letters*, 2022, 120(9):093103.

[20] LIU W J, LIU M L, LIU X M, *et al*.. Recent advances of 2D materials in nonlinear photonics and fiber lasers[J], *Advanced Optical Materials*, 2020, 8 (8):1901631.

[21] QI Y Y, YANG S, WANG J J, *et al*.. Recent advance of emerging low-dimensional materials for vector soliton generation in fiber lasers [J], *Materials Today Physics*, 2022:10622.

[22] LIU Y Z, SUN L, ZHENG B C, et al.. Anisotropic elastic, thermal properties and electronic structures of M_2AlB_2 (M=Fe, Cr, and Mn) layer structure ceramics [J], *Ceramics International,* 2021, 47:1421-1428.

[23] Badie S, Sebold D, Vaßen R, *et al*.. Mechanism for breakaway oxidation of the Ti2AlC MAX phase [J], *Acta Materialia*, 2021, 215:117025.

[24] LEI X, LIN N M. Structure and synthesis of MAX phase materials: a brief review [J], *Critical Reviews in Solid State and Materials Sciences,*2021, 47(5): 736-771.

[25] LIU G T, LI Z F, GAO W H, et al.. Oxidation mechanism and mechanical properties of substitutional transition metal modified Nb4AlC3: A first-principles density functional theory study [J], *Ceramics International*, 2023, 49(17): 29141-29154.

[26] Tallman D J, Anasori B, Barsoum M W, *et al*..A critical review of the oxidation of Ti_2AlC, Ti_3AlC_2 and Cr_2AlC in air[J], *Materials Research Letters*, 2013, 1 (3):115-125.

[27] Barsoum M W, *et al*..The $M_{n+1}AX_n$ phases: A new class of solids[J], *Prog Solid St Chem,* 28, 2000, 28 (1-4):201-281.

[28] Low I M. Advances in Science and Technology of $M_{n+1}AX_n$ Phases[M].Woodhead Publishing, (2012).

[29] Eklund P, Beckers M, Jansson U, *et al*.. Hoegberg H, Hultman L, The $M_{(n+1)}AX_n$ phases: Materials science and thin-film processing[J], *Thin Solid Films*, 2010, 518(8):1851-1878.

[30] JHANG W L, LI C J, WANG A S, *et al*.. Tunable Optical Property of Plasmonic-Polymer Nanocomposites Composed of Multilayer Nanocrystal Arrays Stacked in a Homogeneous Polymer Matrix, 2020, 12(46):5.

[31] Ching W Y, Mo Y, Aryal S, *et al.*. Intrinsic mechanical properties of 20 MAX-phase compounds[J], *Journal of the American Ceramic Society*, 2013, 96 (7):2292-2297.

[32] ZHAO ZH Y, DU B J, REN Z H, *et al.*. Two-Dimensional Nb_4AlC_3 (MAX) and Nb_4C_3 (MXene): Excellent Optical Limiting Materials with Oppositely Applicated Waveband[J], *ACS Appl. Nano Mater*, 2024, 7(3):2775-2785.

[33] Kumar P， Dey A, Roques J,et al. Photoexfoliation Synthesis of 2D Materials[J], ACS Materials Letters, 2022,4(2).

[34] SHI Y M, LI H N, LI L J, *et al.*. Recent advances in controlled synthesis of two-dimensional transition metal dichalcogenides via vapour deposition techniques[J], *Chemical Society Reviews*, 2015, 44 (9):2744-2756.

[35] Jawaid A, Nepal D, Park K, *et al.*. Vaia R A, Mechanism for Liquid Phase Exfoliation of MoS_2[J], *Chemistry of Materials*, 2015, 28(1): 337-348.

[36] LI L CH, ZHOU M, LONG J, *et al.*. Green Preparation of Aqueous Graphene Dispersion and Study on Its Dispersion Stability [J], *Frontiers in Materials*, 2020,13(18):4069.

[37] Harun S W, Lim K S, Ahmad H, *et al.*. Investigation of dispersion characteristic in tapered fiber[J], *Laser Physics*, 2011, 21(5):945-947.

[38] JIANG X W, LV W H, XU Y, *et al.*. Kerr lens mode locked operation in an erbium-doped fiber laser modulated by silica tapered fiber[J], *Optical Fiber Technology*, 2024, 84:103725.

[39] HONG ZH F, ZHANG M X, JIANG X W, *et al.*. Generation of soliton molecules in mode-locked erbium-doped fiber laser by InSb saturable absorber[J], *Infrared Physics & Technology*, 2023,129:104540.

[40] HU CH F, LI F Z, ZHANG J, W, *et al.*. Nb_4AlC_3: A new compound belonging to the MAX phases[J], *Scripta Materialia*, 2007, 57(10): 893-896.

[41] GUO B, XIAO Q L, WANG SH H, *et al.*. 2D Layered Materials: Synthesis, Nonlinear Optical Properties, and Device Applications[J], *Laser & Photonics Review*, 2018, 13(12): 1800327.

[42] SHANG J CH, ZHAO SH ZH,LIU Y ZH. Separation and amplification of Kelly sidebands and main soliton pulse in a 2-μm ultrafast fiber chirped pulse amplifier [J], Infrared Physics & Technology, 2022, 127:104455.

[43] YI J, DU L, LI J, *et al.*. Mochalin, ZHAO C J, A.M. Rao, Unleashing the potential of Ti_2CT_x MXene as a pulse modulator for mid-infrared fiber lasers[J], *2D Materials*, 2019, 6(4):045038.

[44] FENG J J, LI X H, FENG T C, *et al.*. Harmonic mode-locked Er-doped fiber laser by evanescent field-based MXene $Ti_3C_2T_x$ (T= F, O, or OH) saturable absorber[J], *Annalen der Physik*, 2020, 532 (1):1900437.

[45] HUANG W CH, MA CH Y, LI CH, *et al.*. Highly stable MXene (V_2CT_x)-based harmonic pulse generation[J], *Nanophotonics*, 2020, 9(8):2577.

[46] Ahmad H, KamelyA, Yusoff N, *et al.*. Generation of Q-switched pulses in thulium-doped and thulium/holmium-co-doped fiber lasers using MAX phase (Ti_3AlC_2)[J], *Scientific reports*, 2020, 10 (1):9233.

[47]SUN G Q, FENG M, ZHANG K, *et al.*. Q-Switched and Mode-Locked Er-doped fiber laser based on MAX phase Ti_2AlC saturable absorber[J], *Results in Physics*, 2021, 26:104451.

[48] Lee J, Kwon S Y, Lee J H, *et al.*. Harmonically mode-locked Er-doped fiber laser at 1.3 GHz using a V_2AlC MAX phase nanoparticle-based saturable absorber[J], *Optics & Laser Technology*, 2022, 145:107525.

[49] ZHANG K, FENG M, SUN G P, *et al.*. Q-switched and noise-like mode-locked fiber laser based on ternary transition-metal carbide Nb_2AlC saturable absorber[J], *Optics & Laser Technology*, 2023, 162:109237.

Author biographies:

Liu Xiao-juan (1976-), Dr. Ing., Professor, Shandong University of Technology, School of Physics and Optoelectronic Engineering. Her main research interests are fiber laser, fiber amplifier, ultrafast lasers, microwave photonic filters. E-mail: liuxiaojuansd@163.com

Lu Cheng (1990-), Dr. Ing., Shandong University of Technology, School of Physics and Optoelectronic Engineering. His main research interests are novel low dimensional material ultrafast photonic devices and near-infrared single-mode laser technology. E-mail: luchengcg@163.com